Assessing Age-Related Changes in the Biomechanical Properties of Rabbit Lens Using a Coaligned Ultrasound and Optical Coherence Elastography System

Chen Wu,[1] Zhaolong Han,[1] Shang Wang,[1,2] Jiasong Li,[1] Manmohan Singh,[1] Chih-hao Liu,[1] Salavat Aglyamov,[3] Stanislav Emelianov,[3] Fabrice Manns,[4,5] and Kirill V. Larin[1,2]

[1]Department of Biomedical Engineering, University of Houston, Houston, Texas, United States
[2]Molecular Physiology and Biophysics, Baylor College of Medicine, Houston, Texas, United States
[3]Department of Biomedical Engineering, University of Texas at Austin, Austin, Texas, United States
[4]Ophthalmic Biophysics Center, Bascom Palmer Eye Institute, University of Miami Miller School of Medicine, Miami, Florida, United States
[5]Biomedical Optics and Laser Laboratory, Department of Biomedical Engineering, University of Miami College of Engineering, Coral Gables, Florida, United States

Correspondence: Kirill V. Larin, Department of Biomedical Engineering, University of Houston, 4800 Calhoun Road, 3605 Cullen Boulevard, Room 2028, Houston, TX 77204-5060, USA;
klarin@uh.edu.

CW, ZH, and SW contributed equally to the work presented here and should therefore be regarded as equivalent authors.

Submitted: September 9, 2014
Accepted: January 5, 2015

Citation: Wu C, Han Z, Wang S, et al. Assessing age-related changes in the biomechanical properties of rabbit lens using a coaligned ultrasound and optical coherence elastography system. *Invest Ophthalmol Vis Sci*. 2015;56:1292–1300. DOI:10.1167/iovs.14-15654

Purpose. To evaluate the capability of a novel, coaligned focused ultrasound and phase-sensitive optical coherence elastography (US-OCE) system to assess age-related changes in biomechanical properties of the crystalline lens in situ.

Methods. Low-amplitude elastic deformations in young and mature rabbit lenses were measured by an US-OCE system consisting of a spectral-domain optical coherence tomography (OCT) system coaligned with a focused ultrasound system used to produce a transient force on the lens surface. Uniaxial compressional tests were used to validate the OCE data.

Results. The OCE measurements showed that the maximum displacements of the young rabbit lenses were significantly larger than those of the mature lenses, indicating a gradual increase of the lens stiffness with age. Temporal analyses of the displacements also demonstrate a similar trend of elastic properties in these lenses. The stress-strain measurements using uniaxial mechanical tests confirmed the results obtained by the US-OCE system.

Conclusions. The results demonstrate that the US-OCE system can be used for noninvasive analysis and quantification of lens biomechanical properties in situ and possibly in vivo.

Keywords: lens, biomechanics, optical coherence elastography

The age-related changes in viscoelastic properties of the crystalline lens play an important role in the development of presbyopia, which is the progressive, age-related loss of accommodation of the eye.[1–5] Results of ex vivo studies have shown that the stiffness of crystalline lenses increases with age for animals[6–8] and humans.[4,5,9] The increase in lens stiffness is generally believed to be responsible for the progressive loss of the ability of the lens to change shape, leading to presbyopia. However, our current understanding of the mechanical properties of the lens, their changes with age, and their role in presbyopia is limited, in part due to a lack of technology that allows measurements of the mechanical properties of the lens in situ and in vivo. The location of the crystalline lens inside the eye makes it challenging to measure its mechanical properties in vivo or in situ (i.e., inside the globe). The ability to noninvasively measure mechanical properties of the lens in vivo will also allow direct objective evaluation of the outcomes of surgical techniques to restore accommodation that rely on lens softening, including femtosecond lasers, pharmaceutical agents, or lens replacement with a flexible material.[10–14]

Elastography is an emerging technique that can map the local mechanical properties of tissues.[15–19] Ultrasound elastography (USE) and magnetic resonance elastography (MRE) have experienced rapid development during the past few years as diagnostic tools.[9,16,17] One common principle of these techniques is correlating tissue deformation caused by the external mechanical excitation to tissue elasticity. In previous studies, acoustic radiation force was applied to a microbubble created by laser-induced optical breakdown in the lens.[6,8,9,20] The displacement of the microbubble was measured by ultrasound and used to evaluate lens elasticity. However, this approach is invasive because it requires the formation of microbubbles within the lens. Also, in vivo applications of this approach may be limited due to the relatively low sensitivity of ultrasound imaging. To create a noninvasive and highly sensitive method to assess the mechanical properties of the lens in situ and, potentially, in vivo, we propose to apply acoustic radiation pressure on the lens surface and combine acoustic radiation force and OCT techniques.

The basic feasibility of using Brillouin microscopy to measure the lens bulk modulus both in vitro and in vivo has recently been demonstrated.[21–24] Brillouin microscopy can be implemented using simple instrumentation, but it has a relatively slow acquisition. There is also uncertainty on how to correlate Brillouin shift (modulus) to the classical mechanical description of the tissues (e.g., Young modulus). USE and MRE can assess mechanical properties of tissue but the relatively low spatial resolution of USE and MRE is still a critical limitation for certain applications, particularly for ocular tissues and also for measurements at the cellular level.[25] Optical coherence elastography (OCE) is capable of providing direct and high-resolution assessment of mechanical properties of the tissue and, therefore, could overcome the limitations of these techniques.[19,25,26] Optical coherence elastography employs optical coherence tomography (OCT)-based methods to detect the sample deformation induced by an external force. In comparison to USE and MRE,[18] OCE is able to provide superior spatial imaging resolution, faster acquisition speed, and greater displacement sensitivity.[19,25–29] Recent studies have demonstrated the potential of OCE for tumor detection,[30,31] intravascular plaque detection,[32,33] and cornea elasticity measurements.[34–36] Although OCE has been extensively developed for different applications, including for the elastic properties of isolated ocular tissues, in situ quantitative biomechanical measurement of crystalline lens has been very challenging due to the unique location and the localized environment of the lens. We have previously demonstrated the feasibility of using a cofocused ultrasound-OCE (US-OCE) system for biomechanical assessment of tissue-mimicking phantoms that simulate the crystalline lens.[37] This system combines a pulsed ultrasound system capable of producing an acoustic radiation force on the lens surface and a phase-sensitive OCT system for measuring the lens displacement caused by the acoustic radiation force.

In the present study, the biomechanical properties of rabbit crystalline lenses were assessed in situ by using an US-OCE system. Pilot experiments were performed on the lenses of young and mature rabbits in situ (lens located inside an eye globe). Both the maximum displacement and the relaxation rate of the displacement were analyzed. Also, a model-based reconstruction approach was applied to quantify the viscoelastic properties of the lenses. For validation, uniaxial mechanical compression tests were conducted on the same young and mature rabbit lenses.

Materials and Methods

Experimental Setup

To assess the biomechanical properties of the rabbit lens, a cofocused and colocalized ultrasound and OCE system, termed US-OCE, was developed by combining ultrasound excitation with spectral-domain OCT, as schematically shown in Figure 1a. A single element ultrasound transducer (model ISO305HP; CTS Valpey Corporation, Hopkinton, MA, USA) with a diameter of approximately 12.7 mm and a focal length of approximately 19 mm operating at 3.7-MHz central frequency was employed in the system. A sinusoidal wave with a frequency of 3.7-MHz generated by a function generator (model 80; Wavetek Ltd., San Diego, CA, USA) was gated by a 1.1-ms pulse to produce a one-time burst. The driving signal for the ultrasound transducer was amplified using a 50-dB power amplifier (model 350L; Electronics & Innovation Ltd., Rochester, NY, USA). The acoustic radiation force from the ultrasound wave was used to remotely perturb the anterior surface of the crystalline lens through the cornea and the aqueous humor of the eye.

In the phase-sensitive OCT system, a superluminescent laser diode (model S480-B-I-20; Superlum Diodes Ltd., Carrigtwohill, Ireland) with a central wavelength of approximately 840 nm and a bandwidth of approximately 49 nm was used as the light source. The laser beam was separated and directed to the reference and the sample arms of a Michelson interferometer. The interference of the combined light from these two arms was detected using a high-resolution spectrometer comprised of a grating and a line-scanning CCD camera (model L104-2k; Basler, Inc., Ahrensburg, Germany). The A-line acquisition rate of this system was set to be 25 kHz during the experiments. The full width at half maximum (FWHM) of the transverse Gaussian profile of the OCT beam at the imaging focal plane was approximately 8 μm. The system's phase stability measured by recording the interference from the reflection of the two surfaces of a glass slide placed in the sample arm was approximately 4 milliradians. More details of this OCT system setup can be found in our previous publications.[34,37,38]

A custom-built transducer holder was used to securely attach the ultrasound transducer to the OCT objective lens. Coalignment of the focal zone of the ultrasound beam and the OCT imaging beam was achieved by aligning the mounted ultrasound transducer with a needle tip.[37] Acoustic radiation force excitation and OCT M-mode imaging (rapidly repeated A-scans at the same location) were synchronized by a computer-generated triggering signal.

The surface of the crystalline lens was placed at the coaligned focal zone of the US-OCE system. Stimulation with the acoustic radiation force produced a perturbation on the lens surface, resulting in a displacement of the lens surface. The displacement of the apex of the crystalline lens as shown in Figure 1b was measured by the phase-sensitive OCT system. Since the ultrasound pulses were delivered through one part of the cornea, outside of the optical path of the OCT beam, the displacement of the cornea did not contribute significantly to the measured signal from the lens surface.

Sample Preparation

Eyes from young (2- to 3-months old) and mature (over 6-months old) rabbits (Pel-Freez Biologicals, LLC, Rogers, AR, USA) were used in this study. Immediately after enucleating, the globes were shipped overnight in a saline-filled glass container, placed on the ice in a thermo-insulated box (without freezing). All experiments were performed immediately after receiving the eyes. During the experiments, the entire eye globes were kept in the saline solution at room temperature to minimize any change in the tissue properties. The lenses were carefully checked to verify that they are optically clear during experiments. The sample was positioned in a custom-designed eye holder to prevent motion during the experiment. For the US-OCE experiments, three young and four mature rabbit eyes were used. An additional five mature rabbit eyes were used for the uniaxial compressional experiments, thus totaling three young and nine mature eyes.

All experiments adhered to the tenets of the Declaration of Helsinki, to the ARVO Statement for the Use of Animals in Ophthalmic and Visual Research and complied with the University of Houston Institutional Animal Care and User Committee guidelines.

Kinematic Model of the Relaxation Process

The vertical movement of the tissue in the focal zone of the US-OCE, shown as a red dot in Figure 1b, can be separated into forced motion in response to the acoustic radiation push, and

Investigative Ophthalmology & Visual Science

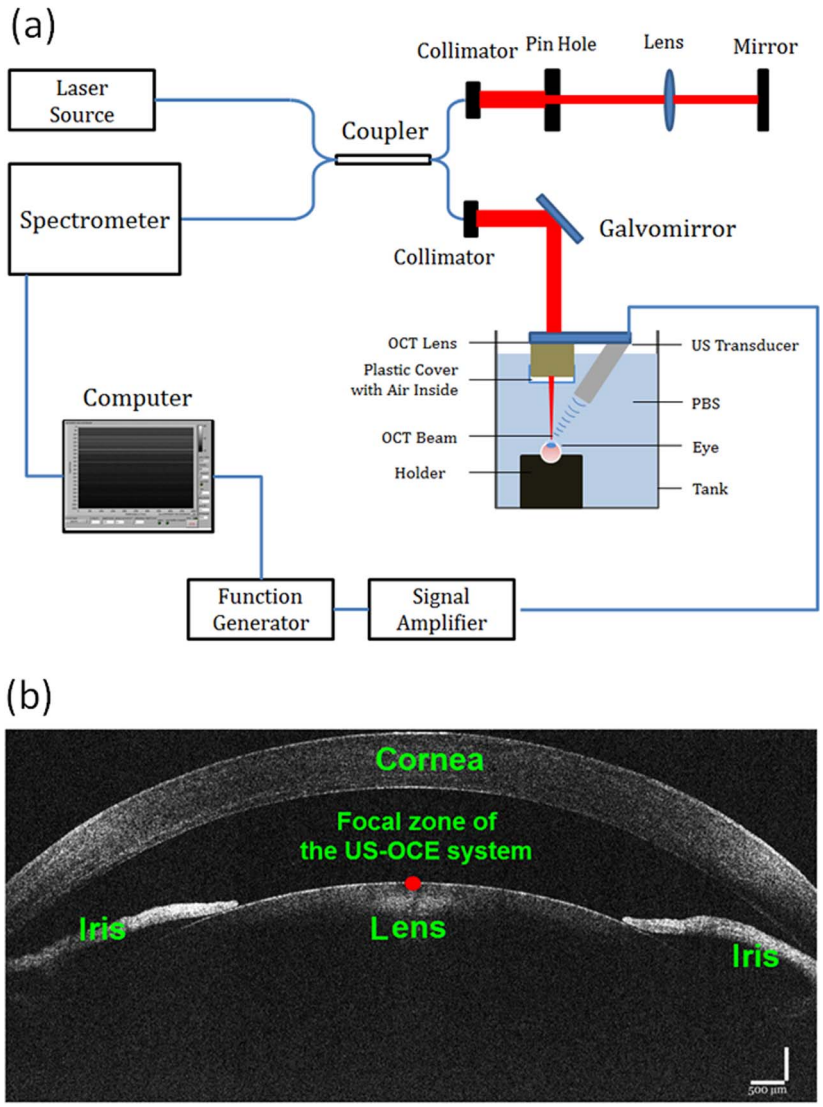

Figure 1. (**a**) Schematic of the coaligned US-OCE system; (**b**) typical OCT image of the rabbit lens.

relaxation motion that occurs after the acoustic radiation force is removed and when the external forces are zero.

The following simplified kinematical differential equation can be used to describe the lens's relaxation process starting from the maximum displacement point:

$$m\frac{d^2y(t)}{dt^2}+c\frac{dy(t)}{dt}+ky(t)=0 \qquad (1)$$

where m is the equivalent mass, c is the viscosity coefficient and k is the equivalent spring stiffness.[22] To understand the basic characteristics of the equation, two parameters, ξ and ω, are introduced where $\xi = c/(2\sqrt{mk})$ is the damping ratio and $\omega = \sqrt{k/m}$ is the undamped natural frequency of the dynamic system. Equation 1 then becomes

$$\frac{d^2y(t)}{dt^2}+2\xi\omega\frac{dy(t)}{dt}+\omega^2y(t)=0 \qquad (2)$$

The analytical solution of Equation 2 is related to the value of ξ as:

1. $y(t)=A(1+Bt)e^{-\omega t}$ when $\xi=1$;
2. $y(t)=e^{-\xi\omega t}(A\cos\omega_D t+B\sin\omega_D t)$ with $\omega_D=\omega\sqrt{1-\xi^2}$ when $0<\xi<1$; and
3. $y(t)=e^{-\xi\omega t}(Ae^{-\omega_D t}+Be^{\omega_D t})$ with $\omega_D=\omega\sqrt{\xi^2-1}$ when $\xi>1$.

Here, A and B are the parameters to be determined. According to the exponent forms of the solution of Equation 2, ω can also be described as the relaxation rate, which corresponds to the rate of the exponential-type displacement recovery process.

Model for a Viscoelastic Layer

To quantitatively evaluate age-related changes in the viscoelastic properties of the rabbit lenses, we considered a model-based reconstructive approach based on the OCE-measured vertical displacement of a homogeneous viscoelastic layer in response to an acoustic radiation force of short duration.[39,40] In this approach, tissue is modeled as an incompressible viscoelastic (Voigt body) layer. An acoustic impulse is considered to be an axisymmetric force applied to the upper surface of the medium in the direction of the z-axis of the cylindrical system of coordinates (r, θ, z). The mechanical parameters: Young's modulus (E), shear viscosity modulus (η),

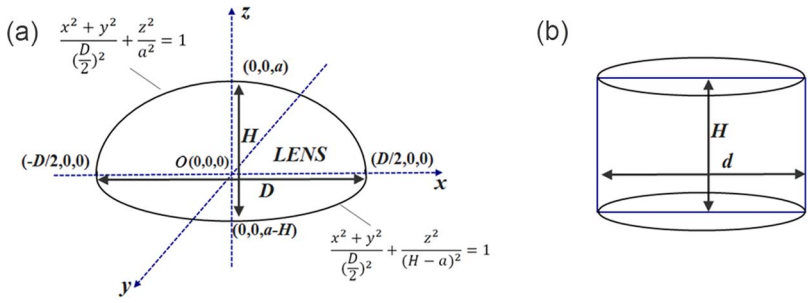

Figure 2. (**a**) Schematic and mathematical description of the rabbit lens shape; (**b**) a transformed cylinder with the same volume as the rabbit lens.

and density (ρ) are constant in the layer. An analytical solution of the spectral component of the vertical displacement in the frequency domain can be derived[39,40]:

$$Y_z(r,z) = -\int_0^\infty \alpha^2 J_0(\alpha r)[A_1 e^{-\alpha z} - A_2 e^{\alpha z} + \alpha(B_1 e^{-\vartheta z} + B_2 e^{\vartheta z})]d\alpha, \quad (3)$$

$$\vartheta = \sqrt{\alpha^2 - k^2}, k^2 = \rho\varpi^2/(E/3 + i\varpi\eta),$$

where J_0 and J_1 are Bessel functions of order 0 and 1, respectively, and ϖ is the angular frequency. Four unknown constants A_1, A_2, B_1, and B_2 are defined using four boundary conditions at the layer boundaries. We consider fixed boundary conditions for the displacements on the bottom of the layer; no shear force on the top surface, and a normal force at the focal point of the transducer. The solution in the time domain was calculated using the inverse Fourier transform after taking into account the duration of the acoustic pulse.

Using the analytical solution of the forward problem (Equation 3), reconstruction of Young's modulus and shear viscosity was posed as a minimization problem, that is by minimizing the error function defined as the difference between the OCE-measured vertical displacement y^{exp} and theoretically calculated displacements y^{theory} at the point ($r = 0$, $z = 0$)[41]:

$$\delta = ||y^{exp} - y^{theory}(E,\eta)||. \quad (4)$$

The density of the lens was assumed to be approximately 1100 kg/m.[3,24,42,43] To minimize Equation 4, a gradient-based iterative procedure was implemented. In the minimization procedure, normalized displacement profiles were used so that only the temporal characteristics of the vertical displacements were taken into account, not the amplitudes. This approach avoided the influence of the ultrasound beam attenuation and differences in acoustic impedance of the materials such as lens and aqueous humor.

Uniaxial Mechanical Compression Tests

After the measurements by the US-OCE system, the eye globes were carefully dissected to extract crystalline lenses for testing with a uniaxial mechanical compression testing system (Model 5943; Instron Corp., Norwood, MA, USA). The lens was centrally positioned between the compression plates of the device. Prior to the mechanical testing on each lens, a 0.004 N preloading force was applied. The compression speed was set to 2 mm/minute. The testing was stopped when the vertical displacement reached 30% the whole thickness. Due to the irregular shape of the lens, it was difficult to directly measure the elasticity based on the conventional compression test method. Thus, an equal-volume transformation method was adopted to calculate the stress-strain relationship.

As shown in Figure 2a, the two parameters of the rabbit lens, height H, and the maximum diameter D, were manually measured with a vernier caliper before the compression test. The volume of the lens was divided into two regions: the upper region, which is above the x-o-y plane, and the lower region which is below the plane. Each part can be simplified as a half ellipsoid, so the upper region can be described by the following formula $x^2 + y^2/(D/2)^2 + z^2/a^2 = 1$, while the lower part is described as $x^2 + y^2/(D/2)^2 + z^2/(H-\alpha)^2 = 1$. The whole volume of the lens can then be estimated by the integration

$$\begin{aligned} V &= V_1 + V_2 \\ &= \int_0^a \pi\left(\frac{D}{2}\right)^2\left(1 - \frac{z^2}{a^2}\right)dz \\ &\quad + \int_0^{H-a} \pi\left(\frac{D}{2}\right)^2\left(1 - \frac{z^2}{(H-a)^2}\right)dz \\ &= \frac{1}{6}\pi HD^2 \end{aligned} \quad (5)$$

To estimate the stress-strain relationship of the lens, a cylinder with height H and diameter d, which has the same volume as the lens, was required (Fig. 2b). Using the equal-volume equation $V = \pi Hd^2/4$, the cylinder diameter d can be calculated as $d = \sqrt{6D/3}$. Using this equation, the stress and strain can be calculated as $\sigma = 4F/(\pi d^2) = 6F/(\pi D^2)$ and $\varepsilon = L/H$, respectively, where F is the external uniaxial mechanical loading, and L is the compressional deformation. The stress-strain curve was then fitted by the empirical exponent formula

$$\sigma = M(e^{N\varepsilon} - 1) \quad (6)$$

where M and N are the parameters to be determined. For each deformation curve, M and N were obtained by using the curve fitting toolbox in MATLAB (Version 2010a, MathWorks, Inc., Natick, MA, USA). The Young's modulus can be calculated by taking the derivative $E = d\sigma/d\varepsilon = MNe^{N\varepsilon}$.

Results

The first parameter used to assess the age-related changes in biomechanical properties of the rabbit lens was the amplitude of the vertical displacements as measured by US-OCE. Figure 3a shows the temporal vertical displacement profiles of typical young and mature lenses. It is clear from either profile that the surface of the crystalline lens starts to deform upon application of the acoustic radiation force. After the removal of the acoustic radiation force, the surface of the lens begins to recover to its original position. Based on the high displacement sensitivity of US-OCE, a minimal acoustic radiation force is sufficient to obtain measurable displacements. Here, the vertical displacement is on the scale of micrometers, which

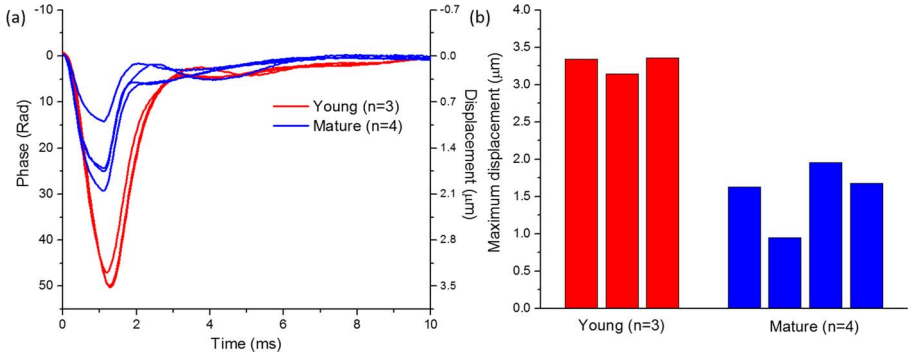

Figure 3. (**a**) Temporal vertical displacement profiles of young ($n = 3$) and mature lenses ($n = 4$) measured by the OCE; (**b**) maximum displacements of the young ($n = 3$) and mature ($n = 4$) lenses.

helps ensure that the structural and functional properties of the crystalline lens are not affected. The data presented in Figure 3b clearly demonstrate a significant difference between the maximum vertical displacements of the young and the mature lenses, which are 3.3 ± 0.1 and 1.6 ± 0.4 μm, respectively. It can be clearly seen that under the same experimental conditions, the maximum vertical displacement of the young lenses is greater than that of the mature lenses, which indicates that the mature lenses are stiffer than the young lenses.

The undamped natural frequencies $\omega = \sqrt{(k/m)}$ of the lenses are shown in Figure 4. The recovery process in each of the phase profiles, which is defined as the range between the maximal displacement point and the starting point of equilibrium, was fitted with our model, as shown in Figure 4a. During the curve fitting process, it was found that the damping ratio, ξ, was greater than 0.99. The damping ratio was therefore, approximated to be equal to 1 for all the lenses. We also evaluated the over-damped model ($\xi > 1$) by fitting the data with formula (c) and confirmed our observation that the surface response is not over-damped. Hence, the formula $y(t) = A(1 + Bt)e^{-\omega t}$ was employed to analyze the relaxation process. Figure 4b shows a comparison of, the undamped natural frequency, ω, for the two age groups. The undamped natural frequency values of the young and the mature lenses are 0.8 ± 0.2 and 2.2 ± 0.5 kHz, respectively. In addition to the maximum vertical displacements, the undamped natural frequencies indicate that the stiffness of the mature lenses is greater than that of the young lenses.

Figure 5 presents a comparison of the vertical displacements measured by OCE at the surface of young and mature lenses and the surface displacements calculated using the model of a viscoelastic layer with mechanical properties found using the error minimization procedure. Note, that only time characteristics of the vertical displacements were used. The amplitudes were not taken into account. To match theoretical and experimental displacement profiles, the acoustic pressure at the focal point of the ultrasound transducer in the theoretical model was set to 15 Pa for both for young and mature lenses. While the acoustic radiation pressure was not directly measured experimentally, it was likely the same in all experiments regardless of the animal age. Similarly, the amplitude of the pressure at the lens surface was assumed to be the same for all eyes in the theoretical model. Interestingly, the maximum vertical displacement in the young lens was approximately twice the value obtained in the mature lens both in the experimental and in theoretical results. However, the reconstruction results show that the Young's modulus of the young lens is three times larger than that of the mature lens. In the mature lens, experimental and theoretical profiles demonstrate saturation of the vertical displacement at the end of the acoustic pulse, which occurs when the elastic response of the medium compensates for the acoustic force. These results are in agreement with our previous results, where acoustic radiation force was used to move laser-induced microbubbles produced in crystalline lenses.[6,20]

The result of the reconstruction of Young's modulus and shear viscosity for young and mature lenses is shown in Figure 6. While there was a significant increase in the Young's modulus with age, the increase of shear viscosity was less pronounced. These results are in agreement with our previous results for bovine lenses, where age-related changes in elastic properties were more pronounced than changes in viscous properties.[6]

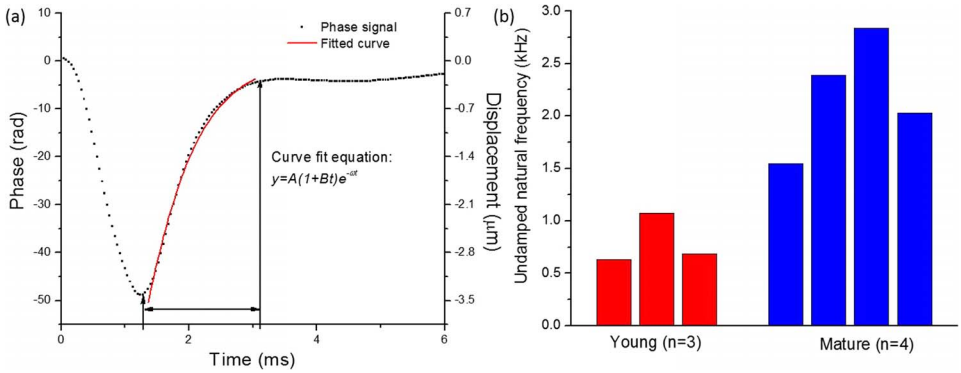

Figure 4. (**a**) Recovery process fitted by $y(t) = A(1+Bt)e^{-\omega t}$ in the OCE-measured vertical displacement; (**b**) the undamped natural frequencies ω for the young ($n = 3$) and mature ($n = 4$) lenses.

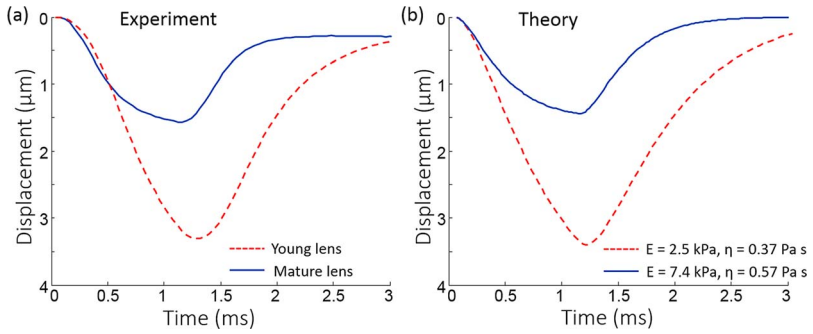

Figure 5. Typical experimentally OCE-measured (**a**) and theoretically calculated (**b**) displacements on the lens surface for young and mature lenses. Theoretically calculated displacements are calculated for viscoelastic parameters E and η obtained after the minimization procedure: $E = 2.5$ kPa and $\eta = 0.37$ Pa·s for young lens, and $E = 7.4$ kPa and $\eta = 0.57$ Pa·s for mature lens.

The stress–strain curves and the Young's moduli of the young and the mature lenses are compared in Figure 7. Figure 7a shows typical examples of the stress-strain curves measured on the young and mature rabbit lenses by uniaxial mechanical compression testing. The stress–strain curves for the young and mature lenses can be fitted as $stress = 0.1928(e^{12.28\times strain} - 1)$ and $stress = 0.11982(e^{16.83\times strain} - 1)$, respectively, where stress is in units of 'kPa'. At a strain of 0.1, Young's moduli of the young ($n = 9$) and mature lenses ($n = 4$) are 8.2 ± 1.1 and 12.6 ± 1.2 kPa, respectively, as shown in Figure 7b. This result clearly shows that the mature lenses are stiffer than the young lenses, confirming the US-OCE results. Also note that the 30% deformation included the deformation caused by the 0.004 N preload. In the calculation of the stress–strain curves, the deformation caused by preload was excluded (thus, the strains shown in Fig. 7a were less than 0.3).

Discussion

In this study, the biomechanical properties of young and mature rabbit crystalline lens were assessed noninvasively using an US-OCE system. The US-OCE system could detect the differences in elastic properties of young and mature rabbit lenses. The analysis of the maximum displacements and undamped natural frequencies as well as the model-based reconstruction of the lens mechanical properties showed that the stiffness of the lens increases with age. Results from the model-based reconstruction indicated an approximately 3-fold increase of Young's modulus in the mature lenses in comparison with the young lenses. This study demonstrates the effectiveness and feasibility of the noninvasive US-OCE method in assessing the biomechanical properties of the lens.

The axis of the OCT beam and, therefore, the direction of the measured displacements were orthogonal to the lens surface. However, the ultrasound transducer was placed at an angle of approximately 45° relative to the OCT sample beam, so that the acoustic radiation force includes both an axial (i.e., vertical or along the axis of the OCT beam) and a transverse component. In our experiment, only the axial displacement at the apical position of the lens surface was measured by the US-OCE system. In general, the measured axial displacements are related to the stiffness gradient inside the lens, including the cortex and nucleus.[37] Our measurements reflect the elastic properties of the whole lens where higher elasticity leads to smaller maximum displacement.

During the experiment, the distance between the sample and the ultrasound transducer was held constant. Therefore, the acoustic radiation force applied on the lens surface can be considered to be approximately the same for all the samples, which eliminates the influence of the magnitude of the acoustic radiation force on the measured lens surface displacement-amplitude.

The undamped natural frequency was extracted from the relaxation process of the lens surface after the excitation by acoustic radiation force was removed. The undamped natural frequency is associated with the elasticity of the sample.[44] The results show that the young lenses had a lower undamped natural frequency than the mature lenses. The analysis of the undamped natural frequency, like the analysis of the maximum surface displacements, therefore shows that the mature lenses are stiffer than the young lenses.

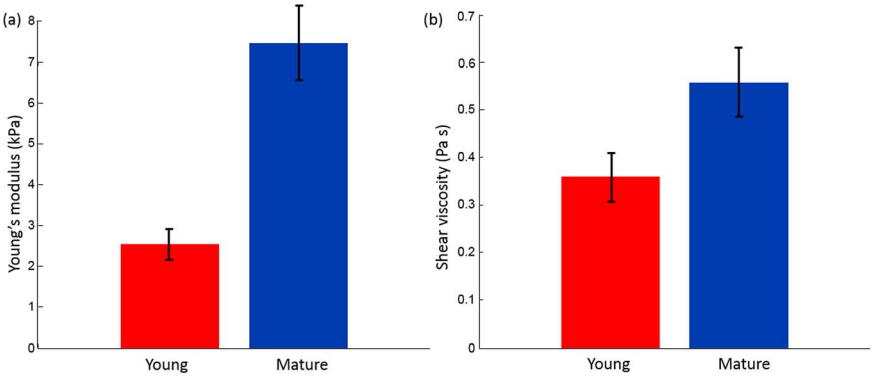

Figure 6. (**a**) Young's modulus and (**b**) shear viscosity modulus of young ($n = 3$) and mature ($n = 4$) lenses estimated based on the model of the viscoelastic layer.

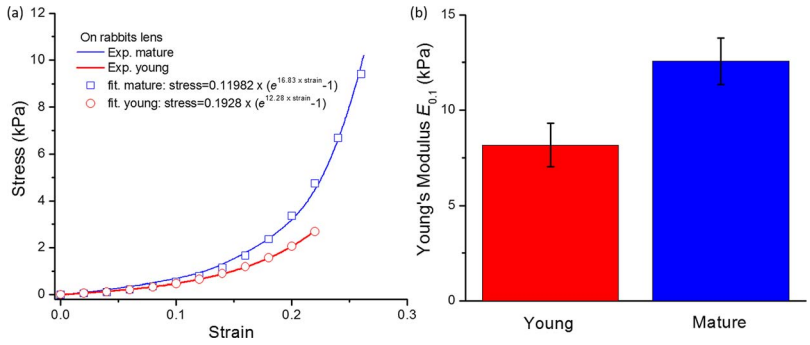

Figure 7. (**a**) Uniaxial mechanical tests and fitted stress-strain curves for typical young and mature rabbit lenses; (**b**) the distribution of the Young's modulus $E_{0.1}$ at strain $\varepsilon = 0.1$ for the young ($n = 9$) and mature ($n = 4$) rabbit lenses.

The relaxation process is mainly associated with the viscoelastic properties of the lens.[37] Small oscillations during the recovery process were observed in both the young and mature lenses, as a result of dynamic processes in the lens after the rapidly applied force. Modeling these processes could result in more accurate quantification of lens biomechanical properties.

In our experiment the undamped natural frequency for the mature rabbit lens was approximately 2 to 3 kHz, while for the young rabbit lens it was approximately 0.6 to 1 kHz. In previous work, it was determined that the undamped natural frequency of the human cornea is approximately 3 kHz,[44] which is of the same order as the undamped natural frequencies of the mature lens measured in the present study. More studies are underway to understand the influence of the lens gradient, viscoelasticity, and age on the relaxation rate and the amplitude of the displacement profile.

It should be noted that there is a high variability in the mature samples for both the elasticity measurements by US-OCE and uniaxial mechanical compression testing. This high variability may imply that the effect of age on the lens elasticity varies between individuals.

Quantitative measurements of the mechanical properties of the crystalline lens based on US-OCE system require the development of an appropriate mechanical model and reconstructive procedure. Here, we have presented a reconstruction approach based on the simplified model of an isotropic homogeneous viscoelastic layer, although in reality the lens has different density distributions and the central nucleus region is harder than the cortex region. In this work, we did not study the gradient density distribution within the lens, and we treated the whole lens as a homogenous object for simplification. This simplification could be one important reason for differences between the uniaxial compression and US-OCE–derived values. Results of the reconstruction demonstrated an approximately 3-fold increase of Young's modulus and 50% increase in shear viscosity in the mature lenses in comparison with the young lenses. This trend agrees with our previous findings, in which a bubble-based acoustic radiation force was applied to measure the elasticity change in porcine and bovine lenses of different ages.[8,20] Furthermore, our quantification of Young's moduli of the rabbit lens using OCE falls in the elasticity range reported for crystalline lens.[4,9,45,46] The US-OCE method presented in this study, which combines acoustic radiation force excitation and phase-sensitive OCT measurement has the advantage of noninvasive detection. Only a minimal acoustic radiation force is required to induce a detectable deformation due to the high displacement sensitivity of phase-resolved OCT detection. This small acoustic radiation helps to preserve the structural and functional properties of the ocular tissues.

Ziebarth et al.[47] investigated the elasticity of the monkey lens by atomic force microscopy. They produced a small indentation approximately 0.5 to 1 μm on the whole in vitro lens and obtained an average Young's modulus of 1.7 kPa, which was close to the 2.5 kPa obtained by OCE and the viscoelastic layer model. The slight disagreement may be due to the source of the lenses, animal species, and method of indentation.

The equal-volume transforming method for reconstructing the stress-strain curves was developed to conform to the requirements of the uniaxial mechanical testing instrumentation. The uniaxial compressional test instrumentation requires that the tested object has the same transverse dimension over the whole object. The crystalline lens, with its spheroid shape, does not meet this requirement. It is therefore impossible to directly derive the stress-strain curves of the crystalline lens. To use the compression test method as well as to facilitate calculation, the simplified equal-volume transforming method, which transforms the lens to a cylinder of equal volume, was developed to estimate the elasticity of the samples.

The initial strain (at strain = 0) was not selected to calculate the Young's modulus because the strain induced during the OCE experiments is not the initial strain. The IOP in the OCE experiments produce a prestress on the rabbit lens, which induces a prestrain. Therefore, Young's modulus in the OCE experiments differs from the Young's modulus obtained from the initial part of the stress-strain curve. Thus, the initial range, (the strain from 0–0.05), was not used for the calculation of the Young's modulus. In this study, IOP was not controlled. The influence of IOP on the elasticity of the lens will be investigated in future work.

As shown in Figure 5, the results of the model-based calculations are in good agreement with the experimental data. However, the reconstructed Young's modulus values are lower than we expected based on the results of uniaxial mechanical compression tests and our previous data obtained in bovine lenses.[6] The underestimation in the elastic modulus could be a result of several limitations in the current model. We believe that the OCE results were determined and influenced by the combined effect of the cortex and nucleus inside the lens. The extent of influence of the nucleus on the results may be different between OCE and uniaxial compression measurement. Even though the crystalline lens is an inhomogeneous object, we have modeled the lens as a homogeneous layer. Therefore, the reconstruction results may correspond to the cortex of the lens, which is softer than the nucleus.[6,8,9] In addition, the effect of the aqueous humor on the displacement of the lens surface was not taken into account. A free boundary condition was assumed for the lens surface. The presence of the aqueous may result in a loss of acoustic energy and underestimation of Young's modulus. Several other factors,

such as motion of the lens as a whole, influence of the lens capsule, and spatial distribution of acoustic pressure at the focal zone were not considered in the model, but may be critical for elasticity reconstruction. The impact of these factors on the estimation of lens elasticity can evaluated by further development of a more sophisticated model of the lens and surrounding tissue that takes into account these effects, together with the use of inverse solution methods.

In this study, the maximal displacements, undamped natural frequencies, model-based reconstruction, and uniaxial mechanical compression tests all clearly indicate that the stiffness of the rabbit crystalline lens increases with age. Prospective future work would be to correlate the relaxation process with a quantitative evaluation of the lens elasticity and to perform depth-resolved OCE measurements to map the elasticity gradient as a function of depth. These studies would allow a better understanding of the internal biomechanical properties of the lens. The proposed US-OCE method could also be potentially used for the in situ mechanical assessment of other types of ocular tissues, such as the ciliary muscle, since these structures could be well resolved using OCT.[48,49]

In summary, the US-OCE system, which combines acoustic radiation force excitation and phase-sensitive OCT, was demonstrated as a promising tool for noninvasive assessment of the age-related changes in the biomechanical properties of the crystalline lens in situ. The high displacement sensitivity of phase-resolved OCT detection enables the measurement of sub-micron displacements on the lens surface, which is critical for future in vivo study as it allows for the application of a minimal acoustic radiation force to induce a detectable displacement and minimizes the potential ultrasound damage to the eye.[50] In addition, the high spatial resolution of OCT allows highly-localized investigation of the mechanical properties of the lens.[29] These features may result in future translation of this technique in clinical applications.

Acknowledgments

Supported by the National Institutes of Health Grants R01EY022362 and R01EY014225 (Bethesda, Maryland, United States).

Disclosure: **C. Wu**, None; **Z. Han**, None; **S. Wang**, None; **J. Li**, None; **M. Singh**, None; **C.-H. Liu**, None; **S. Aglyamov**, None; **S. Emelianov**, None; **F. Manns**, None; **K.V. Larin**, None

References

1. Charman WN. The eye in focus: accommodation and presbyopia. *Clin Exp Optom*. 2008;91:207–225.
2. Glasser A, Campbell MCW. Presbyopia and the optical changes in the human crystalline lens with age. *Vision Res*. 1998;38: 209–229.
3. Glasser A, Croft MA, Kaufman PL. Aging of the human crystalline lens and presbyopia. *Int Ophthalmol Clin*. 2001;41: 1–15.
4. Heys KR, Cram SL, Truscott RJW. Massive increase in the stiffness of the human lens nucleus with age: the basis for presbyopia? *Mol Vis*. 2004;10:956–963.
5. Pau H, Kranz J. The increasing sclerosis of the human lens with age and its relevance to accommodation and presbyopia. *Graef Arch Clin Exp*. 1991;229:294–296.
6. Yoon S, Aglyamov S, Karpiouk A, Emelianov S. The mechanical properties of ex vivo bovine and porcine crystalline lenses: age-related changes and location-dependent variations. *Ultrasound Med Biol*. 2013;39:1120–1127.
7. Reilly M, Ravi N. Microindentation of the young porcine ocular lens. *J Biomech Eng*. 2009;131:044502.
8. Erpelding TN, Hollman KW, O'Donnell M. Mapping age-related elasticity changes in porcine lenses using bubble-based acoustic radiation force. *Exp Eye Res*. 2007;84:332–341.
9. Hollman KW, O'Donnell M, Erpelding TN. Mapping elasticity in human lenses using bubble-based acoustic radiation force. *Exp Eye Res*. 2007;85:890–893.
10. Glasser A. Restoration of accommodation: surgical options for correction of presbyopia. *Clin Exp Optom*. 2008;91:279–295.
11. Ripken T, Oberheide U, Fromm M, Schumacher S, Gerten G, Lubatschowski H. FS-Laser induced elasticity changes to improve presbyopic lens accommodation. *Graef Arch Clin Exp*. 2008;246:897–906.
12. Lubatschowski H, Schumacher S, Fromm M, et al. Femtosecond lentotomy: generating gliding planes inside the crystalline lens to regain accommodation ability. *J Biophotonics*. 2010;3: 265–268.
13. Schumacher S, Oberheide U, Fromm M, et al. Femtosecond laser induced flexibility change of human donor lenses. *Vision Res*. 2009;49:1853–1859.
14. Mello GHR, Krueger RR. Femtosecond laser photodisruption of the crystalline lens for restoring accommodation. *Int Ophthalmol Clin*. 2011;51:87–95.
15. Sarvazyan A, Hall TJ, Urban MW, Fatemi M, Aglyamov SR, Garra BS. An overview of elastography-an emerging branch of medical imaging. *Curr Med Imaging Rev*. 2011;7:255–282.
16. Sinkus R, Daire JL, Vilgrain V, Van Beers BE. Elasticity imaging via MRI: basics, overcoming the waveguide limit, and clinical liver results. *Curr Med Imaging Rev*. 2012;8:56–63.
17. Garra BS. Imaging and estimation of tissue elasticity by ultrasound. *Ultrasound Quarterly*. 2007;23:255–268.
18. Muthupillai R, Lomas DJ, Rossman PJ, Greenleaf JF, Manduca A, Ehman RL. Magnetic-resonance elastography by direct visualization of propagating acoustic strain waves. *Science*. 1995; 269:1854–1857.
19. Kennedy BF, Liang X, Adie SG, et al. In vivo three-dimensional optical coherence elastography. *Opt Express*. 2011;19:6623–6634.
20. Yoon S, Aglyamov S, Karpiouk A, Emelianov S. A high pulse repetition frequency ultrasound system for the ex vivo measurement of mechanical properties of crystalline lenses with laser-induced microbubbles interrogated by acoustic radiation force. *Phys Med Biol*. 2012;57:4871–4884.
21. Scarcelli G, Yun SH. In vivo Brillouin optical microscopy of the human eye. *Opt Express*. 2012;20:9197–9202.
22. Scarcelli G, Kim P, Yun SH. In vivo measurement of age-related stiffening in the crystalline lens by Brillouin optical microscopy. *Biophys J*. 2011;101:1539–1545.
23. Bailey ST, Twa MD, Gump JC, Venkiteshwar M, Bullimore MA, Sooryakumar R. Light-scattering study of the normal human eye lens: elastic properties and age dependence. *IEEE T Bio-Med Eng*. 2010;57:2910–2917.
24. Reiss S, Burau G, Stachs O, Guthoff R, Stolz H. Spatially resolved Brillouin spectroscopy to determine the rheological properties of the eye lens. *Biomed Opt Express*. 2011;2:2144–2159.
25. Kennedy BF, Kennedy KM, Sampson DD. A review of optical coherence elastography: fundamentals, techniques and prospects. *IEEE J Sel Top Quantum Electron*. 2014;20:272–288.
26. Qi W, Chen R, Chou L, et al. Phase-resolved acoustic radiation force optical coherence elastography. *J Biomed Opt*. 2012;17: 110505.
27. Kennedy KM, Ford C, Kennedy BF, Bush MB, Sampson DD. Analysis of mechanical contrast in optical coherence elastography. *J Biomed Opt*. 2013;18:121508.

28. Wang RKK, Kirkpatrick S, Hinds M. Phase-sensitive optical coherence elastography for mapping tissue microstrains in real time. *Appl Phys Lett*. 2007;90:164105.
29. Sun CR, Standish B, Yang VXD. Optical coherence elastography: current status and future applications. *J Biomed Opt*. 2011;16:043001.
30. Liang X, Oldenburg AL, Crecea V, Chaney EJ, Boppart SA. Optical micro-scale mapping of dynamic biomechanical tissue properties. *Opt Express*. 2008;16:11052–11065.
31. Kennedy KM, Es'haghian S, Chin LX, McLaughlin RA, Sampson DD, Kennedy BF. Optical palpation: optical coherence tomography-based tactile imaging using a compliant sensor. *Opt Lett*. 2014;39:3014–3017.
32. Rogowska J, Patel NA, Fujimoto JG, Brezinski ME. Optical coherence tomographic elastography technique for measuring deformation and strain of atherosclerotic tissues. *Heart (British Cardiac Society)*. 2004;90:556–562.
33. Qi WJ, Li R, Ma T, Shung KK, Zhou QF, Chen ZP. Confocal acoustic radiation force optical coherence elastography using a ring ultrasonic transducer. *Appl Phys Lett*. 2014;104:123702.
34. Wang S, Larin KV. Shear wave imaging optical coherence tomography (SWI-OCT) for ocular tissue biomechanics. *Opt Lett*. 2014;39:41–44.
35. Li J, Wang S, Singh M, et al. Air-pulse OCE for assessment of age-related changes in mouse cornea in vivo. *Laser Physics Letters*. 2014;11:065601.
36. Li J, Han Z, Singh M, Twa MD, Larin KV. Differentiating untreated and cross-linked porcine corneas of the same measured stiffness with optical coherence elastography. *J Biomed Optics*. 2014;19:110502–110502.
37. Wang S, Aglyamov S, Karpiouk A, et al. Assessing the mechanical properties of tissue-mimicking phantoms at different depths as an approach to measure biomechanical gradient of crystalline lens. *Biomed Opt Express*. 2013;4:2769–2780.
38. Wang S, Sherlock T, Salazar B, et al. Detection and monitoring of microparticles under skin by optical coherence tomography as an approach to continuous glucose sensing using implanted retroreflectors. *IEEE Sens J*. 2013;13:4534–4541.
39. Aglyamov S, Shang W, Karpiouk A, et al. Assessment of the depth-dependence of the mechanical parameters of a layered medium using surface excitation and motion measurements on the surface. *Ultrasonics Symposium (IUS), 2013 IEEE International*. Prague: IEEE; 2013:1252–1255.
40. Aglyamov S, Wang S, Karpiouk A, Li J, Emelianov S, Larin KV. Model-based optical coherence elastography using acoustic radiation force. *Proc SPIE*. 2014;89460T–89468T.
41. Aglyamov SR, Skovoroda AR, Xie H, et al. Model-based reconstructive elasticity imaging using ultrasound. *Int J Biomed Imaging*. 2007;2007:35830.
42. Vaughan J, Randall J. Brillouin scattering, density and elastic properties of the lens and cornea of the eye. *Nature*.1980;284:489–491.
43. Su X, Vesco C, Fleming J, Choh V. Density of ocular components of the bovine eye. *Optom Vis Sci*. 2009;86:1187–1195.
44. Han Z, Tao C, Zhou D, et al. Air puff induced corneal vibrations: theoretical simulations and clinical observations. *J Refract Surg*. 2014;30:208–213.
45. Kikkawa Y, Sato T. Elastic properties of the lens. *Exp Eye Res*. 1963;2:210–215.
46. Weeber HA, Van Der Heijde RG. Internal deformation of the human crystalline lens during accommodation. *Acta Ophthalmol*. 2008;86:642–647.
47. Ziebarth NM, Wojcikiewicz EP, Manns F, Moy VT, Parel JM. Atomic force microscopy measurements of lens elasticity in monkey eyes. *Mol Vis*. 2007;13:504–510.
48. Lossing LA, Sinnott LT, Kao C-Y, Richdale K, Bailey MD. Measuring changes in ciliary muscle thickness with accommodation in young adults. *Optom Vis Sci*. 2012;89:719.
49. Buckhurst H, Gilmartin B, Cubbidge RP, Nagra M, Logan NS. Ocular biometric correlates of ciliary muscle thickness in human myopia. *Ophthalmic Physiol Opt*. 2013;33:294–304.
50. Duck FA. Medical and non-medical protection standards for ultrasound and infrasound. *Progr Biophys Mol Biol*. 2007;93:176–191.

Investigative Ophthalmology & Visual Science